IEEE Open Access Journal of
Power and Energy

Received 22 November 2021; revised 15 March 2022; accepted 4 May 2022.
Date of publication 13 May 2022; date of current version 31 May 2022.

Digital Object Identifier 10.1109/OAJPE.2022.3175129

Optimal Controllers to Improve Transient Recovery of Grid-Following Inverters Connected to Weak Power Grids

THILINI HATHIYALDENIYE[1] (Member, IEEE), CHANDANA KARAWITA[2] (Senior Member, IEEE), BAGEN BAGEN[1,3] (Senior Member, IEEE), NALIN PAHALAWATHTHA[4] (Member, IEEE), AND UDAYA D. ANNAKKAGE[1] (Senior Member, IEEE)

[1]Department of Electrical and Computer Engineering, University of Manitoba, Winnipeg, MB R3T 2N2, Canada
[2]Transgrid Solutions Inc., Winnipeg, MB R3T 6C2, Canada
[3]Manitoba Hydro, Winnipeg, MB R3C 0G8, Canada
[4]Hatch Ltd., North Sydney, NSW 2060, Australia

CORRESPONDING AUTHOR: T. HATHIYALDENIYE (hathitmk@myumanitoba.ca)

This work was supported in part by Mitacs, in part by Manitoba Hydro, and in part by the Natural Sciences and Engineering Research Council of Canada (NSERC) under Reference RGPIN-2016-05892.

ABSTRACT

Leading to the enormous growth in renewable and power electronics technologies and the global drive towards environmental friendliness and sustainability, a significant number of renewable energy sources are being connected to the power system via inverter-based systems. The inverter-based generations (IBG) have no stored energy and less fault current injection capability compared to the conventional synchronous machines. Consequently, a large penetration of IBG creates challenges to maintaining the stability of the power system, especially the transient stability. The weaker the power system, the higher the significance of instability. Few solutions exist in the literature to improve the fault recovery of IBG connected to weak power systems. This paper considers the method of storing energy in sub-module capacitors of the Modular-Multi-level Converter (MMC) along with temporarily boosting the inverter's current limit. Conversely, increasing the ratings of the inverter will result in high manufacturing costs. Hence an optimization strategy is proposed in this paper, for obtaining a robust set of inverter control parameters that enhances fault recovery without excessively increasing the manufacturing cost of MMC. A frequency scanning technique supplemented with Generalized Nyquist criteria is incorporated into the optimization methodology to constrain the search space for the optimization algorithm. This enables the optimization algorithm to converge to an acceptable solution with a reasonable computing time. Furthermore, validation of the resultant set of parameters for different system conditions is presented. Finally, IBG with optimized fault recovery controllers is integrated into a simplified real-world power system, and the applicability of the proposed optimized controllers is illustrated.

INDEX TERMS Energy storage, fault recovery, frequency scanning, IBG, inertia emulation, inverter controls, MMC, power electronics converter, stability.

I. INTRODUCTION

CONVENTIONAL power systems contain hydro, fossil and nuclear generations that are fully dispatchable, controllable, and those generator units have large rotating masses. The high rotating inertia of the synchronous generator (SG) provides the capability to store or release kinetic energy in the presence of frequency deviation. It minimizes the active power imbalance allowing the grid to keep the frequency very close to its nominal value and enhancing the frequency dynamics [1]. If the power system fails to maintain the frequency within acceptable limits owing to a rapid loss of generators or load shedding, it can affect the overall stability of the power system, and could result in fault cascades and blackouts. The renewable energy sources are connected to the grid via power electronic converters, which do not have the same inertia as SG-turbine sets. Therefore, increasing the penetration of renewable sources reduces the power system's rotational inertia, resulting in high-frequency deviations, large power swings, and a high Rate Of Change Of Frequency (ROCOF). These concerns will have a negative impact on power system stability, and could cause the power system to become unstable [1]–[4].

Furthermore, the SG is capable of driving the field current to its ceiling during a severe fault like a three-phase fault. The high current injection feature enables the SG to release the stored energy back to the system as soon as the fault is cleared without compensating reactive power supply, accordingly recovering voltage and frequency quickly. Power electronic inverters can only boost their current up to the maximum current rating of the power electronic switches, which is typically around 1.1pu. As a result, the current handling capability of these inverter-based generations (IBG) is less compared to SGs [5].

Several approaches for mitigating the limitations of IBG have been proposed in the literature. One way is changing the ROCOF withstand capability of the power system. However, this method does not address the inertia issue [6]. Another solution is employing a backup SG with a partial load as a spinning reserve or a synchronous condenser. This method offers rotational inertia, which enhances power system stability, yet, it comes with high capital and operating costs. The most prevalent method in the literature is to provide synthetic inertia through virtual synchronous machines. Numerous variations of this approach have been published since it was first proposed in [7]. In this method, synchronous machine equations are incorporated in the inverter controls to emulate the initial response of the synchronous machines. Capacitors or/and energy storage systems are required in most virtual inertia methods, to provide/absorb the active power necessity of the grid. The virtual inertia methods can be divided into three primary categories, which are as follows:

1) Synchronous generator model-based methods This method comprises synchronous machine equations to determine electrical and mechanical parameters, including virtual torque, excitation, flux equations and virtual impedance at various depths. There are several subcategories available depending on the synchronous machine model utilized, such as synchronverters [8], [9], Virtual Synchronous Machine (VISMA) Topology [7], Institute of Electrical Power Engineering (IEPE) Topology [10], Kawasaki Heavy Industries (KHI) Lab's Topology [11]. These methods have the ability to regulate voltage, frequency, active and reactive power. The key advantage of most of these methods is that they do not rely on ROCOF as input; hence, the concerns with ROCOF measurements can be avoided. Furthermore, these methods provide accurate synchronous machine models that are consistent with electromechanical transient studies. Moreover, these methods consist of a frequency-drooping mechanism along with real power regulation which helps to reduce power-frequency oscillations. There are few drawbacks, such as no intrinsic over current protection owing to the usage of voltage source model and numerical instability issues [1], [7]–[16].

2) Swing equation-based methods These typologies employ the power-frequency swing equation, instead of the complete comprehensive model of SG, reducing the complexity compared with SG model-based approaches. Such methods are found in the literature as Ise Lab's Topology [17], [18] and Synchronous Power Controller (SPC) [19], [20]. These techniques do not have a frequency-drooping mechanism, and also damping and inertia are two parameters that need to be tuned compared to SG model-based methods. Consequently, these techniques might cause power frequency oscillation thus, proper tuning of the control parameters is essential. Voltage source model is utilized in these topologies, similar to the first category, and thereby do not have built-in over-current protection [1], [15]–[20].

3) Frequency-dependent active power response methods Instead of modelling physical devices (SG or swing equations), these techniques emphasize controlling the inverter. Power-Frequency (P-f) droop controllers, synchronous power controllers, virtual oscillation controllers are the most popular varieties of these techniques. Subcategories of these methods are namely VSYNC's Topology [21], Virtual Synchronous Generators [22], Droop based approach [22], Virtual Oscillator Control (VOC) [23], and Inducverters [24]. These approaches are adaptable and may be used for a broad variety of applications. They are only limited by generating and storage technologies, as well as the capabilities of power converters. These techniques generally leverage current source implementation, which provides intrinsic overcurrent protection. They do, however, require PLL, which may cause instability, and their transient response is slower than the other two categories [1], [15], [16], [21]–[24].

The advantages and disadvantages of the three virtual inertia methods are compared in Table 1.

Reference [25], [26] presented a virtual control method for grid forming inverters and reference [27] for grid following inverters. These three references are all based on Swing equation based methods. These references showed promising results for the grid scenarios they considered; however, all of the limitations discussed under swing equations methods apply to these methods as well.

Synthetic inertia control may be delayed in reacting to grid events due to its measurement and control delays. Thus, even though synthetic inertia approaches are extensively available in the literature, they cannot be considered a perfect substitute for conventional SGs in terms of their efficacy.

Some literature suggests alternative methods for the provision of energy required for synthetic inertia. Such methods are proposed in [28] as Inertia Emulation Control (INEC) and in [29] as Generator Emulation Control (GEC), which supply energy using dc-link capacitors. Large DC capacitors are expected for these techniques to deliver the requisite synthetic inertia while preserving the DC-link voltage. Converter-based technology is moving towards the Modular-Multi-level Converter (MMC) from traditional two-level converters. MMCs do not have a common DC-link capacitor. Instead, each

TABLE 1. Comparison of virtual inertia methods.

Methods	Advantages	Disadvantages
Synchronous generator model based methods	• Use accurate SM models • Not use ROCOF as an input • Use frequency-drooping mechanisms • Do not need PLL	• No intrinsic over current protection • Numerical instability issues
Swing equation-based methods	• Use swing equation model • Simple configuration • Do not need PLL	• No intrinsic over current protection • No frequency drooping mechanism • In-proper tuning might cause Oscillations
Frequency-dependent active power response methods	• Emphasize controlling the inverter • Intrinsic over current protection	• Use of PLL might cause instability • Transient response is slow

sub-module has a capacitor. Therefore, energy storage has to be in those sub-module capacitors.

A method of storing energy in sub-module capacitors by controlling the sub-module capacitor voltage has been proposed in [30]. This approach was enhanced further in [5], [31], [32] by temporarily increasing the current limit of the inverter. The researchers suggested temporarily increasing inverter current limits and sub-module voltages immediately upon the fault detection, to store a significant amount of energy in the sub-module capacitors during the fault. The stored energy is then released upon clearing the fault without any undesirable electromechanical oscillations. The method in [5], [31], [32] has several advantages over the other methods found in the literature. It provides fast energy release upon clearing the fault and no undesired electromechanical oscillations. DC voltage will be retained with minimal fluctuations and high performance can be accomplished even for weak systems. Further, this method does not require ROCOF as an input, unlike most synthetic inertia methods. However, increasing the ratings of the inverter will lead to a significant rise in manufacturing costs. [5], [31], [32] have only presented the concept of this control strategy, but they have not analyzed the optimal setting for best performance considering the dynamic behaviour of the system and the cost factors. As such, this research extends the method proposed in [5], [31], [32] by focusing on obtaining an optimal set of values for the inverter control parameters that provide enhanced fault recovery without excessively increasing the manufacturing cost of the inverter. The frequency analysis technique along with Nyquist stability criteria is also employed, to determine the ranges of PI controller gains that result in stable system dynamics. This is used to constrain the search space in the optimization so that the optimization algorithm can converge to an acceptable solution with reasonable computational time.

The rest of this paper is organized as follows. Section II discusses the theoretical background related to the concept. The methodology combined with details of the test system, controller implementation and optimization is demonstrated in Section III. The results are provided in Section IV together with validation and application to a real-world power system. The Real-Time Digital Simulator platform (RTDS) [33] is used, as the simulation tool for this research. Finally, recommendations and conclusions are given in Section V.

II. THEORETICAL BACKGROUND

This research aims at determining the best configurations for inverter controllers to recover from faults in a way comparable to synchronous machines and at the same time without having to unduly increase the manufacturing cost of inverters. Two key aspects must be considered to achieve better fault recovery using IBG, as described in [5], [31], [32]. The first aspect is the ability of IBG to store energy during the fault to offer inertia support to the system, and the second aspect is the ability of IBG to temporarily raise its current limit to allow a fast flow of energy once the fault is cleared.

A. ENERGY STORAGE

Synchronous machines consist of directly coupled spinning masses, that can store and restore energy during frequency aberrations, thereby overcoming supply and demand imbalances. It is known as the inertial response of the synchronous machine, and it aids the power system in achieving a more efficient fault recovery process [1]. Therefore, the ability to store and release energy in the occurrence of system faults is a key aspect for IBG to gain a similar fault recovery response as SG.

Renewable energy sources can generate power continuously unless they are disconnected from the grid during faults. Thus, if they remain linked and store their energy somewhere rather than sending it to the grid during the fault, the stored energy can be utilized to rapidly recuperate from faults. The energy storing method considered for this research is the method of storing energy in the inverter sub-modules, similar to that of [5], [31], [32].

A fixed number of capacitors are switched on per arm (total of upper and lower arm sub-modules) during the normal operation of MMC. The total voltage across these sub-module capacitors equals the DC voltage as given in (1) with the assumptions of the voltage drop across arm inductors is negligible and sub-module capacitor voltages are balanced.

$$V_{DC} = N_{SM}.V_{SM} \tag{1}$$

where; V_{DC} is the DC voltage, N_{SM} is the total number of sub-modules switch on, and V_{SM} is the voltage across a sub-module capacitor.

This method maintains a constant DC voltage, and therefore if the total number of sub-modules that are switched on decreases, then the sub-module voltage has to be increased to preserve the same DC voltage according to (1). The increase in sub-module capacitors' voltage will cause more energy

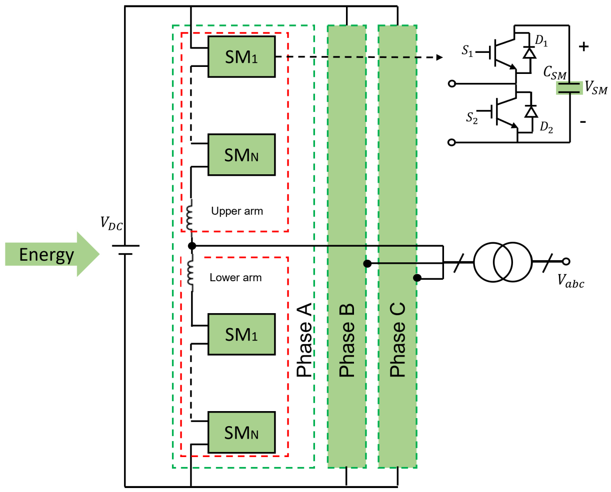

FIGURE 1. **Energy storage in inverter sub-modules.**

to be stored inside the sub-module capacitors. Similarly, if the number of sub-modules switched on is increased, the sub-module voltage will decrease to maintain constant DC voltage; hence the sub-module capacitors can release the stored energy back to the system. Fig. 1 presents a simple MMC configuration. During a transient event, the energy from the rectifier side is stored in the inverter's sub-module capacitors, which are highlighted in green in Fig. 1.

Energy stored in a Sub-module capacitor (E_{SM}):

$$E_{SM} = \frac{1}{2} C_{SM} V_{SM}^2 \tag{2}$$

Total energy accumulated in the inverter:

$$\triangle E_{Total} = \triangle E_{SM} N_{SM} N_{poles} N_{arms} \tag{3}$$

where; C_{SM} is the size of the sub-module capacitor, N_{poles} is the number of poles and N_{arms} is the number of arms.

B. HIGH TRANSIENT CURRENT

High current injection capability is the next important aspect of the synchronous machine that aids in fault recovery. SGs can boost their terminal current by more than three times the nominal current during faults. As a result, synchronous machines can provide the required active power to maintain frequency stability without compensating the reactive power supply during the recovery period. The power system is therefore competent in preserving both voltage and frequency stability.

The MMC is not designed to have a high current rating, and in most cases, the maximum allowed inverter current is only about 1.1pu. IBG must prioritize reactive current as soon as the fault is cleared to compel with the grid codes to promote voltage stability. However, this will result in a decrease in the active power supply, causing frequency instability. Design of a temporarily increased high current rating for a short period would probably be more cost-effective than a moderately high current rating for a long period. This research, thus, aims to establish optimal current and span for better fault recovery when all the above-mentioned factors are minimized.

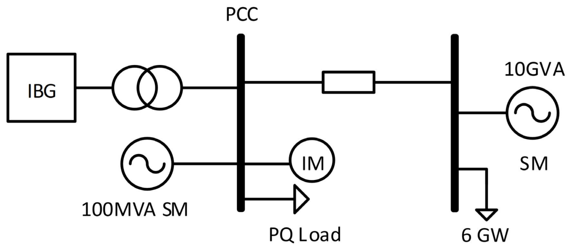

FIGURE 2. **Test system.**

III. METHODOLOGY

This research focuses primarily on optimization to obtain an optimal set of inverter control parameters to produce enhanced fault recovery while not excessively increasing the manufacturing cost of inverters. Further, a frequency scanning technique is incorporated in optimization to narrow the search space of the optimization and thus achieve an acceptable solution within reasonable computing time. A detailed description of the test system and the technique employed are provided in this section.

A. TEST SYSTEM

The test system represents a small remote network with IBG and a small SG that feeds electricity to a local load center, as illustrated in Fig. 2. The remote network is connected to a strong AC network via a weak transmission line with a short circuit ratio (SCR) of 1.0. The inverter rating is 500MVA and is designed to operate at maximum active power of 450 MW. The IBG is modelled with a back-to-back MMC-VSC HVDC transmission system. The rectifier is in DC voltage (V_{dc}) and AC voltage (V_{ac}) control mode and the inverter is in active power and V_{ac} control mode. The relevant parameters of the MMC-VSC transmission system are presented in Table 2.

Low inertia (H = 2s) 100MVA SG is used to represent the local synchronous machine-based generation. This low-inertia generator will introduce low damped electromechanical oscillations to the system as an additional challenge for fault recovery. An induction machine and a PQ load are used to depict the load center. The induction machine has a rating of 240MVA and operates at 200MW active power and 4MVar of reactive power. The PQ load is 400MW and 57MVar. The IBG is assumed to be generating at its max capacity (subject to the availability of sun or wind). The difference in power is supplied across the two transmission lines.

B. CONTROLLER IMPLEMENTATION

There are primarily two controllers to be implemented, as stated in section II. The first controller enables energy storage during the fault while the second controller temporally increases the maximum allowable current of the inverter.

TABLE 2. Details of the MMC-VSC transmission system.

DC Voltage	200kV
Converter transformer	230/100kV, 500MVA, X=0.15pu
Number of Sub-modules	110
Sub-module voltage	1.8kV
Sub-module capacitance	10mF
Phase reactance	50mF

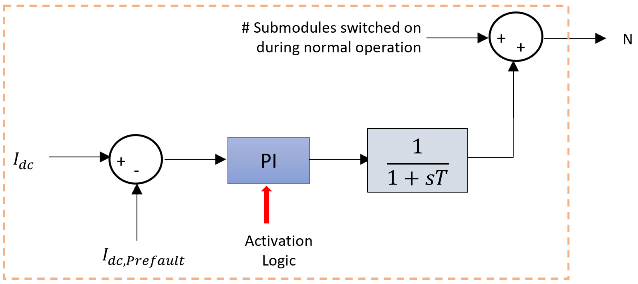

FIGURE 3. Energy storing controller.

1) ENERGY STORING CONTROLLER

In this approach, the active power coming from the renewable source will not be disconnected during the fault, but will be stored in the capacitors of the inverter sub-module. Theoretically, DC power flow should therefore not be impaired by the fault. The energy storage in the inverter sub-modules is accomplished by adjusting the number of sub-modules that are switched on, as stated in section II-A. Thereupon, the DC current can be used as an input measurement for the PI controller that controls the number of sub-modules required to be switched on as shown in Fig. 3.

2) MAXIMUM CURRENT CONTROLLER

The next important factor to consider is the inverter's maximum current limit. The controllers typically limit the inverter current to around 1.1 pu. However, the inverter must be capable of providing a high current for releasing energy during the recovery period to achieve a speedy recovery. This technique, therefore, considers temporarily raising the inverter current limit for a short period to achieve a fast recovery following faults. Literature shows that 100% reactive current priority does not give the best performance [32]. Both the total current magnitude and maximum reactive current limit have a significant influence on fault recovery. Accordingly, the maximum current limit, as well as reactive current limit, are both treated as control parameters.

There are two ways of increasing the current limit. The first approach demands the system to hold a certain high current limit for a specified amount of time. This approach was used in [5], [31], [32], however, it may be placing an undue burden on the inverter, as well as causing the system to become unstable by supplying excessively high current for a high period of time. The method implemented in this research provides the maximum allowable current and the maximum allowable current boosting span. The current controller then determines how much maximum current and span of rising current are

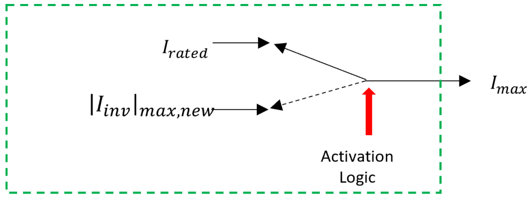

FIGURE 4. Maximum current controller.

required to sustain the stability. When the inverter current requested by the outer loop control exceeds or equals the new maximum current limit, the inverter current is increased to the new maximum current limit. As soon as it drops below the new maximum, the inverter starts to reduce current. However, the duration of increasing the inverter current during a transient event is constrained by the pre-defined maximum duration of increasing current. Instead of using a rigid limit that forces the inverter current to be remain at the maximum limit for a certain duration, the method used here provides improved performance.

The inverter current is calculated using (4) and (5). The current controller used for this method is shown in Fig. 4. The inverter functions at or below its rated current throughout the normal operation; when a fault occurs, the inverter current rises to the new maximum limit for a certain period.

$$I_{q,limited} = \begin{cases} I_{q,max} & I_q \geq I_{q,max} \\ I_q & I_{q,max} > I_q > I_{q,min} \\ I_{q,min} & I_q \leq I_{q,min} \end{cases} \tag{4}$$

$$I_{inv} = \sqrt{I_d^2 + I_{q,limited}^2} \tag{5}$$

3) ACTIVATION LOGIC

The above two controllers should be triggered only during the faults. The voltage of the inverter terminal bus can be reduced due to a fault and also due to high loading situations. Hence, in addition to the inverter terminal voltage, the apparent power at the common coupling bus is considered to be an input indicator for the activation control. When the inverter terminal voltage and load apparent power are both dropped below their pre-set thresholds, the activation logic will be generated for a certain period. This controller permits the system to store energy during the fault and transfer that energy to the system with a high current rating. The overall controller diagram is given in Fig. 5.

C. OPTIMIZATION

This section describes the optimization process used to acquire the optimal set of values for inverter control parameters to achieve improved fault recovery while not excessively increasing the production costs of MMC.

1) DECISION PARAMETERS

Decision parameters are the key parameters that influence the fault recovery and the manufacturing cost of MMC.

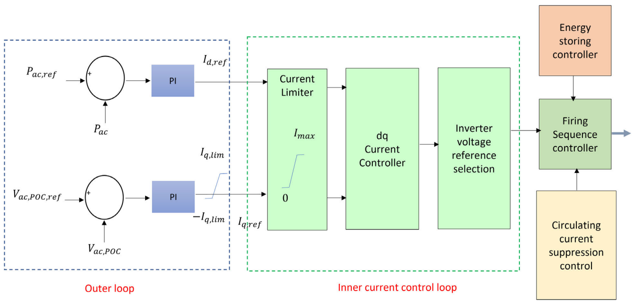

FIGURE 5. Overall controller diagram.

The maximum inverter current, the reactive current limit, and the amount of energy stored in the number of sub-modules impact the fault recovery performance of the system. As explained in section II-A, the amount of energy stored in the sub-modules is dictated by the sub-module voltage, thence the number of sub-modules. The maximum current limit, sub-module voltage, and the duration of increasing the voltage and current of the inverter influence the manufacturing cost of MMC. They must be upheld at minimum levels to minimize production costs, yet those parameters must also be high enough to facilitate enhanced fault recovery. Consequently, it is important to find the optimal values for all of the above parameters, to strike a good compromise between the fault recovery and manufacturing cost.

The maximum inverter current and the maximum reactive current limits are two of the decision parameters. The amount of energy storage in the sub-module capacitors depends on the rise of sub-module voltage and is regulated by changes in the number of active sub-modules. The number of sub-modules is controlled through a PI controller that is used to maintain the DC current at constant. Thus, the parameters of the PI controller (K_P and K_I) are another two decision parameters. Lastly, the duration of changing the number of sub-modules is another decision parameter. As such, those five parameters are identified as the decision parameters for the optimization.

The next step is identifying the constraints for the search space in the optimization. The ranges (upper and lower limits) for K_P and K_I are determined by performing a frequency scanning analysis, as explained in the following section.

2) FREQUENCY SCANNING ANALYSIS TO IDENTIFY THE RANGES OF KP AND KI

Frequency scanning analysis is typically used to analyze the small-signal instability of grid-connected IBG systems. There are various frequency analysis approaches available in the literature [34]–[38]. The DQ-based frequency scanning method is utilized in this study since it is straightforward and only requires two independent scans. The frequency scanning method is used in this research to obtain the range of new PI controller parameters for the optimization that will not cause small-signal instability.

Small signal analysis is valid only in the vicinity of the equilibrium state. After a large disturbance, a stable system from 'large disturbance sense' will reach this equilibrium. However, if it is unstable from small signal sense, it will not settle those. By determining the permissible range of parameters from small signal sense, the overall search space can be eliminated, because there is no point in trying parameters that makes the system unstable around the equilibrium.

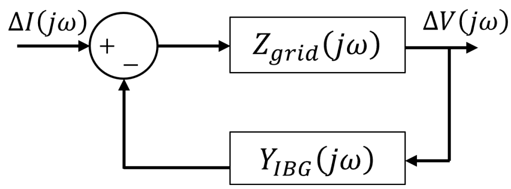

FIGURE 6. Control block diagram of combined grid and IBG systems.

The entire system is represented by two independent systems (IBG system and Grid system) in this DQ analysis approach, and the frequency scanning is performed individually for those two systems. Then the independently obtained frequency scanned results are combined in the frequency domain, as given in (6)-(14) and Fig. 6.

Grid

$$\begin{bmatrix} \Delta V_d(j\omega) \\ \Delta V_q(j\omega) \end{bmatrix} = Z_{grid}(j\omega) \begin{bmatrix} \Delta I_d(j\omega) \\ \Delta I_q(j\omega) \end{bmatrix} \tag{6}$$

$$\Delta V(j\omega) = Z_{grid}(j\omega)\Delta I(j\omega) \tag{7}$$

where;

$$Z_{grid}(j\omega) = \begin{bmatrix} \Delta Z_{dd}(j\omega) & \Delta Z_{dq}(j\omega) \\ \Delta Z_{qd}(j\omega) & \Delta Z_{qq}(j\omega) \end{bmatrix} \tag{8}$$

IBG

$$\begin{bmatrix} \Delta I_d(j\omega) \\ \Delta I_q(j\omega) \end{bmatrix} = Y_{IBG}(j\omega) \begin{bmatrix} \Delta V_d(j\omega) \\ \Delta V_q(j\omega) \end{bmatrix} \tag{9}$$

$$\Delta I(j\omega) = Y_{IBG}(j\omega)\Delta V(j\omega) \tag{10}$$

where;

$$Y_{IBG}(j\omega) = \begin{bmatrix} \Delta Y_{dd}(j\omega) & \Delta Y_{dq}(j\omega) \\ \Delta Y_{qd}(j\omega) & \Delta Y_{qq}(j\omega) \end{bmatrix} \tag{11}$$

According to the Fig. 6,

$$\Delta V(j\omega) = Z_{grid}(j\omega)[\Delta I(j\omega) + Y_{IBG}(j\omega)\Delta V(j\omega)] \tag{12}$$

$$\begin{aligned} \frac{\Delta V(j\omega)}{\Delta I(j\omega)} &= [I + Z_{grid}(j\omega)Y_{IBG}(j\omega)]^{-1}Z_{grid}(j\omega) \\ &= Z_{eq}(j\omega) \end{aligned} \tag{13}$$

Therefore, the closed-loop transfer function is:

$$Z_{eq}(j\omega) = [I + Z_{grid}(j\omega)Y_{IBG}(j\omega)]^{-1}Z_{grid}(j\omega) \tag{14}$$

The stability of the combined system is determined using Generalized (MIMO) Nyquist Criteria (GNC) [34]. Since independent systems are stable, the open-loop system which is $L(s) = Z_{grid}Y_{IBG}$, is also stable. Thence, the number of open-loop unstable poles of the multi-variable system is equal to zero. Hence, according to the GNC, the closed-loop system becomes stable if the net sum of counterclockwise encircles

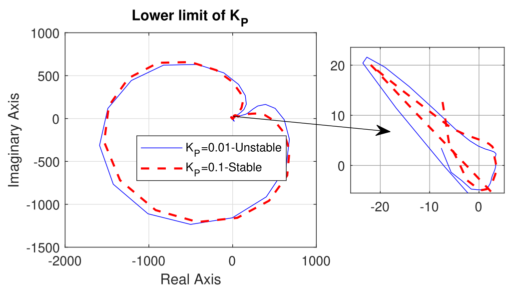

FIGURE 7. Lower limit of K_P.

created around the origin by the Nyquist plot of $det(I+L(s))$ equals zero and does not pass through the origin.

Nyquist plot of $det(I+L(s))$ for four different values of K_P and K_I are given in Fig. 7, Fig. 8, Fig. 9 and Fig. 10. According to Fig. 7, the number of clockwise encircles (N) is formed by the Nyquist plot of $det(I+L(s))$ around the origin when $K_P = 0.01$ equals 1 and the number of counterclockwise encircles (P) equals zero. As a result, the total number of counterclockwise encircles (P-N) around the origin is equal to -1. This implies that the system will be unstable if $K_P = 0.01$. Similarly when $K_P = 0.1$, N = 1 and P = 1, thus the total number of counterclockwise encircles (P-N) equals zero. Moreover, the Nyquist plot does not pass through the origin. Accordingly, the system with $K_P = 0.1$ is stable. Thus, the lower limit for the K_P was chosen to be 0.1.

Similarly, as demonstrated in Fig. 8, the upper limit for the K_P was chosen as 1.45, since the system is stable with $K_P = 1.45$ but not with $K_P = 1.5$.

The system is unstable when $K_I = 0.001$ and stable when $K_I = 0.01$, as presented in Fig. 9. Therefore, the lower limit for the K_I was selected as 0.01.

When $K_I = 30$, the system is stable and when $K_I = 32$ system is unstable, as presented in Fig. 10. Accordingly, the upper limit for the K_I was set to 30.

Feasible operating ranges are considered for other decision variables (I_{max}, $I_{q,ref,limit}$ and $SM_{duration}$). Finally, the lower and upper limits for the decision variables were defined as given in (15)-(19)

$$1.0 \leq I_{max} \leq 1.6 \tag{15}$$
$$0.2 \leq I_{q,ref,limit} \leq 1.3 \tag{16}$$
$$0.1 \leq SM_{duration} \leq 1.5 \tag{17}$$
$$0.1 \leq K_P \leq 1.45 \tag{18}$$
$$0.01 \leq K_I \leq 30 \tag{19}$$

3) OUTPUT MEASURABLE VARIABLES

RMS error, steady-state error, and the maximum overshoot of Inverter active power output, inverter current magnitude, voltage magnitude at the PCC, system frequency, and DC current were considered, as the output measurable variables. The error was evaluated in relation to the pre-fault values since the goal was to swiftly restore the system to the pre-fault values with few overshoots. The weighting factors for each

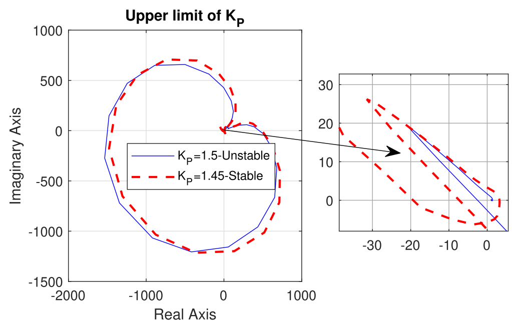

FIGURE 8. Upper limit of K_P.

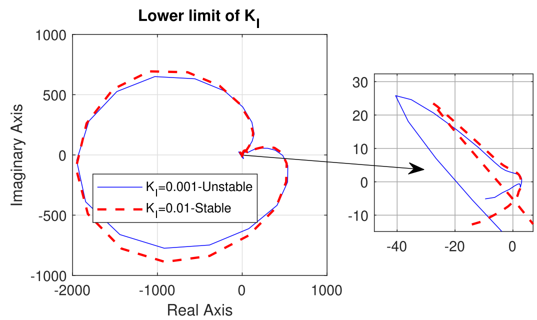

FIGURE 9. Lower limit of K_I.

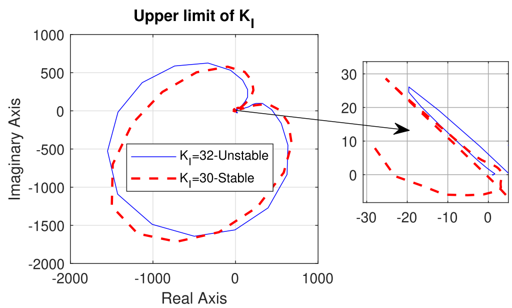

FIGURE 10. Upper limit of K_I.

of the aforementioned variables were chosen so that stable and unstable conditions can be clearly distinguished, and the fundamental goal of storing energy in sub-module capacitors and releasing it was achieved with less change in DC power flow. Accordingly, comparatively high values were used for w_6 to w_{10} to differentiate stable and unstable conditions and for w_5, w_{10} and w_{15} to achieve storing and releasing energy in sub-module capacitors with less change in DC power flow.

The objective function used for this study is given in (20). Optimization was performed to obtain the minimum value of the objective function subjected to eq (15)-(19).

$$OBJ_f = \begin{pmatrix} w_1.PE_{rms} + w_2.VE_{rms} + w_3.fE_{rms} \\ +w_4.IE_{rms} + w_5.IDCE_{rms} + w_6.PE_{ss} \\ +w_7.VE_{ss} + w_8.fE_{ss} + w_9.IE_{ss} \\ +w_{10}.IDCE_{ss} + w_{11}.PE_{os} + w_{12}.VE_{os} \\ +w_{13}.fE_{os} + w_{14}.IE_{os} + w_{15}.IDCE_{os} \end{pmatrix} \tag{20}$$

where; $w_1 - w_{15}$ are weighting factors, E_{rms} is rms error, E_{ss} is steady-state error, E_{os} is the maximum overshoot, P is Inverter active power output, V is voltage magnitude at the PCC, f is

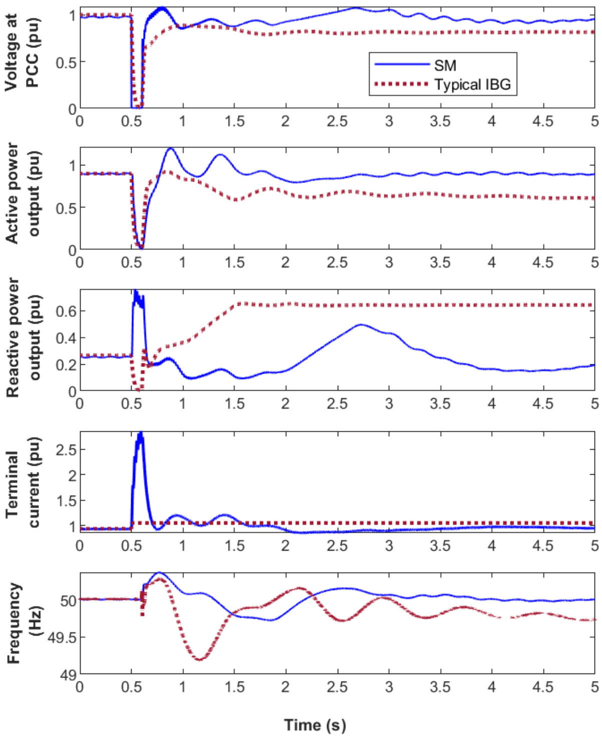

FIGURE 11. Comparison of fault recovery behaviour of synchronous machine and typical IBG.

system frequency, I is inverter current magnitude and IDC is DC current.

This research used the non-linear simplex optimization method [39] for optimization. The set of values corresponding to the minimum cost function with minimum I_{max} and $SM_{duration}$ was selected, as the optimization solution.

IV. RESULTS

A five-cycle three-phase ground fault was applied at the point of common coupling (PCC) to investigate the dynamic behaviour of the system. Fig. 11 depicts a comparison of the dynamic behaviour of the Synchronous Machine vs an IBG system without any special controllers (typical IBG). According to this, the IBG connected to a weak system cannot recover to pre-fault values from the imposed fault, although similar rated SG connected to the same system could. Hence, Fig. 11 insights the necessity of improved fault recovery controllers for the IBGs connected to weak power systems.

A. OPTIMIZATION RESULTS

Table 3 presents the optimal set of inverter control parameters obtained from the optimization to achieve better fault recovery without unduly increasing the manufacturing cost of the inverter. Fig. 12 provides the fault response of the IBG system with this optimal set of parameters. When a fault occurs, the inverter current limit must be increased to 1.35, as specified in Table 3, for approximately 0.5s, as shown in Fig. 12(b). The K_P and K_I values of the PI controller used to change the number of sub-modules are 1.2 and 9, respectively. The duration of changing the number of sub-modules is only 0.5s, as given in Table 3, and the inverter sub-module voltage rises to 4 kV for a very short period (approx. 0.1s). About 45MJ of energy, which is comparable to the same rated SG system, is stored in the inverter sub-module capacitors during the fault and released back to the system as soon as the fault is cleared to obtain a fast recovery, as depicted in Fig. 12(f). Since the reactive current limit is maintained at 0.9pu and the current limit is increased to 1.35pu, the inverter can provide active and reactive power requirements to the system, as presented in Fig. 12(d)&(e). As a result, both PCC voltage and system frequency are restored to pre-fault values with few fluctuations, as shown in Fig. 12(a)&(c). In addition, the inverter maximum current and sub-module voltage are maintained at appropriate values and their boosting periods are about 0.5s. This will result in lower production costs than by offering a high-rated MMC. Accordingly, an IBG equipped with these optimized controllers can provide enhanced fault recovery without unduly increasing inverter manufacturing costs.

TABLE 3. Optimal set of parameters for inverter controls.

Parameter	Value
I_{max}	1.35pu
$I_{q,ref,limit}$	0.9
K_P	1.2
K_I	9
$SM_{duration}$	0.5s

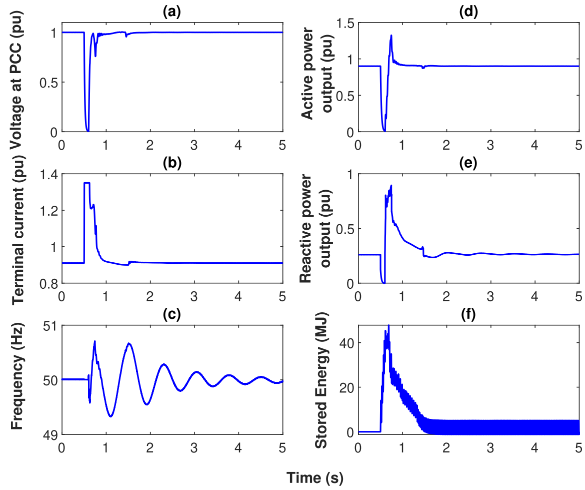

FIGURE 12. IBG with optimized controllers.

The Nyquist diagrams of a typical IBG system and an IBG system with optimized controllers at the post fault stage are compared in Fig. 13. As shown in Fig. 13, the typical IBG system's Nyquist plot of $det(I + L(s))$ forms one clockwise encircle (N) and zero counterclockwise encircles (P) around the origin. As a result, the total number of counterclockwise encircles (P-N) equals -1. This implies that the typical IBG connected to a weak power system is unstable. However, the Nyquist plot of the IBG system with optimized controllers makes one clockwise encircle and one counterclockwise encircle; thence, the total encircles around the origin is zero,

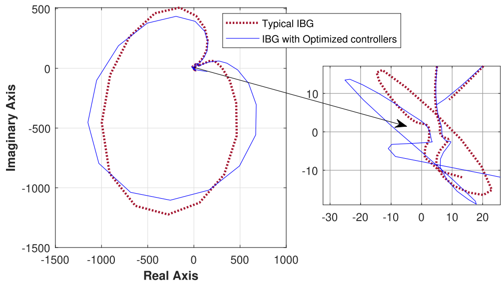

FIGURE 13. **Comparison of Nyquist diagrams of typical IBG vs. IBG with optimized controllers.**

as illustrated in Fig. 13. Therefore, the IBG system with optimized controllers connected to a weak power system is stable.

B. VALIDATION

The parameter optimization was performed at only one system operating point, thus it will not necessarily imply that the given set of parameter values will produce a good performance at other operating points. Hence, the following step is necessary to validate that the optimal set of parameter values give good performance at a range of expected operating points. Therefore a few case studies are offered here, as examples to demonstrate the validation procedure. Control parameters must be re-tuned if the validation does not work, as expected. This is an essential step in the design process.

1) EFFECTS OF LOAD TYPE

The optimal set of parameters was obtained by considering constant MVA load. Thus, constant impedance and constant current loads were used in this study to check if the optimal set of control parameters works regardless of load type. Fig. 14 shows the comparison of system performance (voltage at PCC, inverter current and system frequency) for those three types of loads. Since all three cases provide a similar fault recovery, Fig. 14 verifies that the optimal set of values for the inverter control parameters works irrespective of the load type.

2) EFFECT OF SYSTEM IMPEDANCE

This case study was carried out by altering the transmission line impedance that links the load centre and the remote grid. The change in transmission line impedance represents the changes in network topology due to contingencies. The optimization was done with an impedance magnitude of 294.2Ω (SCR about 1.0). In this case study, the transmission line impedance was changed to different values, and the dynamic performance of the system was observed. Fig. 15 presents the dynamic behaviour of the system for three different impedance values. The impedance of the system could be increased to 420 Ω and achieve a stable and good dynamic response. Increasing system impedance further can make the system unstable. Hence, we recommend identifying the worst system impedance, owing to credible contingencies

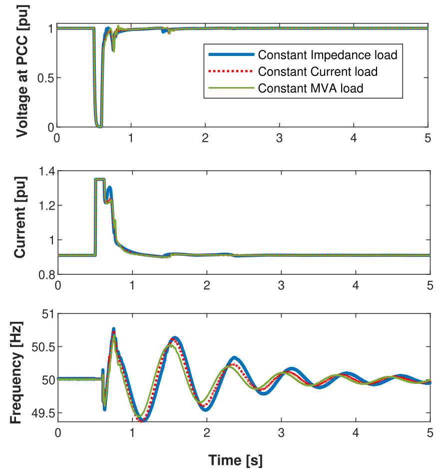

FIGURE 14. **Dynamic performance of the system with different types of loads.**

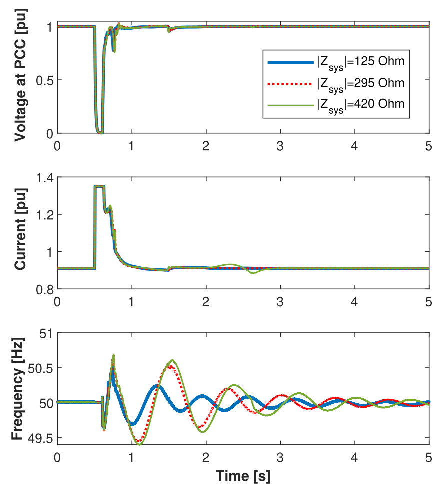

FIGURE 15. **Dynamic performance of the system with different values of transmission line impedance.**

first. If the worst impedance is beyond the operating range of the optimum control parameters, the authors recommend determining another set of inverter control parameters to employ in such instances.

3) EFFECT OF FAULT DURATION

The duration of fault was changed in this case study to observe the impact of fault duration on the dynamic performance. Fig. 16 shows the system behaviour for 4 different values of fault duration. Decreasing fault duration helps with fault recovery, as illustrated in Fig. 16. Fault duration could be increased up to 0.12s (6 cycles) and obtain good recovery following a fault with the optimal set of parameters. However, as shown in Fig. 16, a further increase in fault duration has a negative effect on faults' recovery. Most grid codes for power systems with high penetration of IBG compel zero-voltage ride-through capability of 5-6 cycles at 230kV. Hence these results imply that the optimized set of parameters is capable of satisfying such requirements. If validation fails, control settings must be re-tuned.

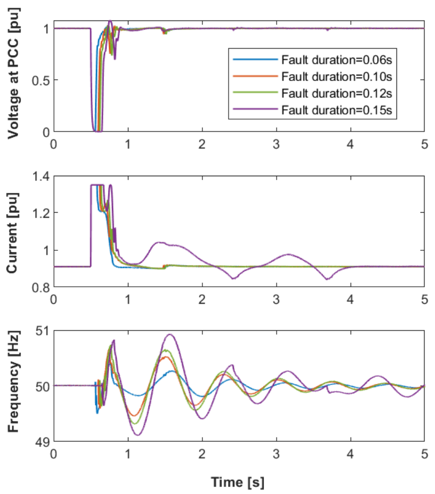

FIGURE 16. **Dynamic performance of the system with different fault duration.**

TABLE 4. **Details of the MMC-VSC transmission system.**

DC Voltage	200kV
Converter transformer	110/200kV, 800MVA, X=0.18pu
Number of Sub-modules	200
Sub-module voltage	2kV
Sub-module capacitance	10mF
Phase reactance	50mF

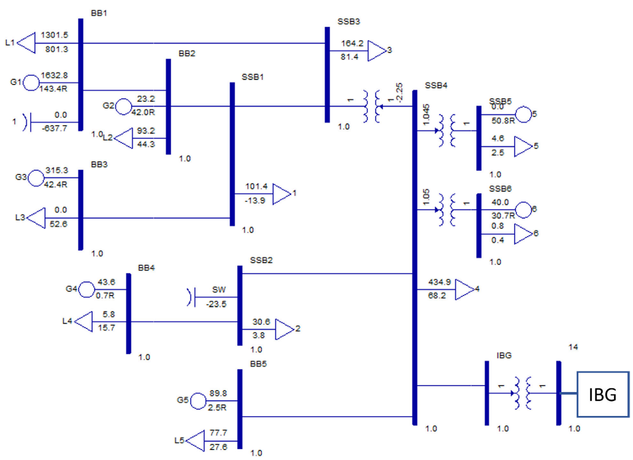

FIGURE 17. **MH dynamically simplified system with IBG.**

C. APPLICATION

IBG with optimized fault recovery controllers was incorporated into the dynamically simplified Manitoba hydro-power system [40] to demonstrate the application of the proposed optimized controllers. The system diagram is given in Fig. 17.

The inverter rating is 800MVA and is designed to operate at maximum active power of 760 MW. The IBG is modelled with a back-to-back MMC-VSC HVDC transmission system, and the rectifier is in DC voltage (V_{dc}) and AC voltage (V_{ac}) control, and the inverter is in active power and V_{ac} control. The important parameters of the MMC-VSC transmission system are presented in Table 4. SCR at the PCC bus (SSB4) is 1.7. The fault recovery controllers employ the same parameter values listed in Table 3.

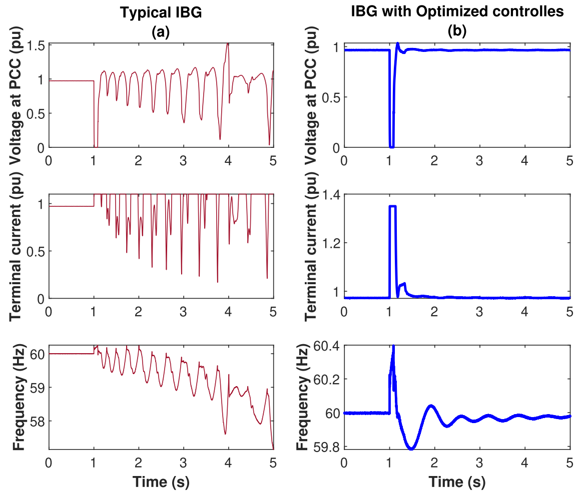

FIGURE 18. **Comparison of fault recovery behaviour of typical IBG system and IBG system with optimized controllers.**

A five-cycle three-phase ground fault was applied at the PCC bus (SSB4) and the dynamic behaviour of the system with and without optimized controllers was observed. The fault responses of the typical IBG and the IBG with optimized controllers are depicted in Fig. 18(a)&(b). According to Fig. 18 a typical IBG system cannot recover from the imposed fault, while the same IBG system with optimized controllers can give enhanced recovery. Accordingly, this emphasizes the importance of the optimized fault recovery controller.

V. CONCLUSION

The importance of auxiliary fault recovery controllers for IBG coupled to weak power systems is highlighted in this paper. The concept of storing energy in the inverter sub-module capacitors and temporarily increasing the inverter current limit to achieve a rapid energy flow is adopted in this paper to enhance the fault recovery of IBG. An optimization methodology is presented in this paper to obtain enhanced fault recovery without excessively increasing the manufacturing cost of MMC. The search space must be appropriately narrowed for the optimization algorithm to converge to an acceptable solution with a reasonable computing time. This is achieved using frequency scanning combined with Generalized Nyquist criteria. In the proposed approach, the inverter current must be boosted to 1.35pu for about 0.5s and energy coming from the rectifier side is stored in inverter sub-module capacitors during the fault. Enhanced performance is achieved with the optimal set of parameter values even for a very weak power system. Furthermore, the optimized parameter values are validated in this paper for various system conditions, as an essential step in the design process. If the validation fails, re-tuning the control parameters is suggested. The application of the optimal inverter control parameters is demonstrated by incorporating the controllers into a dynamically simplified real-world power system.

ACKNOWLEDGMENT

The authors would like to thank Manitoba Hydro for providing technical support.

REFERENCES

[1] B. Hartmann, I. Vokony, and I. Táczi, "Effects of decreasing synchronous inertia on power system dynamics—Overview of recent experiences and marketisation of services," *Int. Trans. Elect. Energy Syst.*, vol. 29, no. 12, 2019, Art. no. e12128.

[2] D. Wu, M. Javadi, and J. N. Jiang, "A preliminary study of impact of reduced system inertia in a low-carbon power system," *J. Mod. Power Syst. Clean Energy*, vol. 3, no. 1, pp. 82–92, Mar. 2015.

[3] U. Agrawal, J. O'Brien, A. Somani, T. Mosier, and J. Dagle, "A study of the impact of reduced inertia in power systems," in *Proc. 53rd Hawaii Int. Conf. Syst. Sci.*, 2020.

[4] A. Ulbig, T. S. Borsche, and G. Andersson, "Impact of low rotational inertia on power system stability and operation," *IFAC Proc. Volumes*, vol. 47, no. 3, pp. 7290–7297, 2014.

[5] M. Annakkage, C. Karawita, and H. Suriyaarachchi, "Voltage and frequency support of modular multilevel converters connected to weak grids," *CIGRE Sci. Eng.*, vol. 15, pp. 94–104, Jan. 2019.

[6] P. Energy, "Rate of change of frequency (ROCOF)-review of TSO and generator submissions final report," Commission Energy Regulation (CER), Tech. Rep., 2013.

[7] H.-P. Beck and R. Hesse, "Virtual synchronous machine," in *Proc. 9th Int. Conf. Electr. Power Quality Utilisation*, Oct. 2007, pp. 1–6.

[8] Q.-C. Zhong and G. Weiss, "Synchronverters: Inverters that mimic synchronous generators," *IEEE Trans. Ind. Electron.*, vol. 58, no. 4, pp. 1259–1267, Apr. 2010.

[9] Q.-C. Zhong, "Virtual synchronous machines: A unified interface for grid integration," *IEEE Power Electron. Mag.*, vol. 3, no. 4, pp. 18–27, Dec. 2016.

[10] Y. Chen, R. Hesse, D. Turschner, and H.-P. Beck, "Improving the grid power quality using virtual synchronous machines," in *Proc. Int. Conf. Power Eng., Energy Electr. Drives*, May 2011, pp. 1–6.

[11] Y. Hirase, K. Abe, K. Sugimoto, and Y. Shindo, "A grid connected inverter with virtual synchronous generator model of algebraic type," *IEEJ Trans. Power Energy*, vol. 132, no. 4, pp. 371–380, 2012.

[12] Q.-C. Zhong and G. Weiss, "Static synchronous generators for distributed generation and renewable energy," in *Proc. IEEE/PES Power Syst. Conf. Expo.*, Mar. 2009, pp. 1–6.

[13] Q.-C. Zhong, P.-L. Nguyen, Z. Ma, and W. Sheng, "Self-synchronized synchronverters: Inverters without a dedicated synchronization unit," *IEEE Trans. Power Electron.*, vol. 29, no. 2, pp. 617–630, Feb. 2014.

[14] P. Piya and M. Karimi-Ghartemani, "A stability analysis and efficiency improvement of synchronverter," in *Proc. IEEE Appl. Power Electron. Conf. Expo. (APEC)*, Mar. 2016, pp. 3165–3171.

[15] U. Tamrakar, D. Shrestha, M. Maharjan, B. P. Bhattarai, T. M. Hansen, and R. Tonkoski, "Virtual inertia: Current trends and future directions," *Appl. Sci.*, vol. 7, no. 7, p. 654, 2017.

[16] K. Y. Yap, C. R. Sarimuthu, and J. M.-Y. Lim, "Virtual inertia-based inverters for mitigating frequency instability in grid-connected renewable energy system: A review," *Appl. Sci.*, vol. 9, no. 24, p. 5300, Dec. 2019.

[17] K. Sakimoto, Y. Miura, and T. Ise, "Stabilization of a power system with a distributed generator by a virtual synchronous generator function," in *Proc. 8th Int. Conf. Power Electron. (ECCE Asia)*, May 2011, pp. 1498–1505.

[18] K. Sakimoto, Y. Miura, and T. Ise, "Stabilization of a power system including inverter type distributed generators by the virtual synchronous generator," *IEEJ Trans. Power Energy*, vol. 132, no. 4, pp. 341–349, Apr. 2012.

[19] P. Rodriguez, I. Candela, and A. Luna, "Control of PV generation systems using the synchronous power controller," in *Proc. IEEE Energy Convers. Congr. Expo.*, Sep. 2013, pp. 993–998.

[20] P. R. Cortés, J. I. C. García, J. R. Delgado, and R. Teodorescu, "Virtual controller of electromechanical characteristics for static power converters," U.S. Patent App. 14 001 853, Mar. 6, 2014.

[21] J. Driesen and K. Visscher, "Virtual synchronous generators," in *Proc. IEEE Power Energy Soc. Gen. Meeting-Convers. Del. Elect. Energy 21st Century*, Jul. 2008, pp. 1–3.

[22] V. Van Thong *et al.*, "Virtual synchronous generator: Laboratory scale results and field demonstration," in *Proc. IEEE Bucharest PowerTech*, Jun. 2009, pp. 1–6.

[23] B. B. Johnson, S. V. Dhople, A. O. Hamadeh, and P. T. Krein, "Synchronization of parallel single-phase inverters with virtual oscillator control," *IEEE Trans. Power Electron.*, vol. 29, no. 11, pp. 6124–6138, Dec. 2014.

[24] M. Ashabani, F. D. Freijedo, S. Golestan, and J. M. Guerrero, "Inducverters: PLL-less converters with auto-synchronization and emulated inertia capability," *IEEE Trans. Smart Grid*, vol. 7, no. 3, pp. 1660–1674, May 2016.

[25] D. Pan, X. Wang, F. Liu, and R. Shi, "Transient stability of voltage-source converters with grid-forming control: A design-oriented study," *IEEE J. Emerg. Sel. Topics Power Electron.*, vol. 8, no. 2, pp. 1019–1033, Jun. 2020.

[26] H. Yu, M. A. Awal, H. Tu, I. Husain, and S. Lukic, "Comparative transient stability assessment of droop and dispatchable virtual oscillator controlled grid-connected inverters," *IEEE Trans. Power Electron.*, vol. 36, no. 2, pp. 2119–2130, Feb. 2021.

[27] H. Wu and X. Wang, "Design-oriented transient stability analysis of grid-connected converters with power synchronization control," *IEEE Trans. Ind. Electron.*, vol. 66, no. 8, pp. 6473–6482, Aug. 2019.

[28] J. Zhu, C. D. Booth, G. P. Adam, A. J. Roscoe, and C. G. Bright, "Inertia emulation control strategy for VSC-HVDC transmission systems," *IEEE Trans. Power Syst.*, vol. 28, no. 2, pp. 1277–1287, May 2013.

[29] H. Alatrash, A. Mensah, E. Mark, G. Haddad, and J. Enslin, "Generator emulation controls for photovoltaic inverters," *IEEE Trans. Smart Grid*, vol. 3, no. 2, pp. 996–1011, Jun. 2012.

[30] S. Debnath and M. Chinthavali, "Control of MMC-HVDC in low-inertia weak grids," in *Proc. IEEE 12th Int. Conf. Power Electron. Drive Syst. (PEDS)*, Dec. 2017, pp. 435–441.

[31] M. S. Annakkage, C. Karawita, H. Suriyaarachchi, and U. D. Annakkage, "Control of VSC to emulate the inertia support of a synchronous machine," in *Proc. 15th IET Int. Conf. AC DC Power Transmiss. (ACDC)*, 2019, p. 5.

[32] M. Annakkage, C. Karawita, H. Suriyaarachchi, and U. Annakkage, "Coordinating voltage, inertia, frequency and power oscillation damping support of a VSC HVDC connected to a weak grid," in *Proc. CIGRE Symp.*, Aalborg, Denmark, 2019, pp. 1–11.

[33] *RSCAD—Power System Simulation Software*. Rtds Technologies, Winnipeg, MB, 2021, Canada.

[34] S. Skogestad and I. Postlethwaite, *Multivariable Feedback Control: Analysis and Design*, vol. 2. 2007.

[35] M. K. Das, A. M. Kulkarni, and P. B. Darji, "Comparison of DQ and dynamic phasor based frequency scanning analysis of grid-connected power electronic systems," in *Proc. Power Syst. Comput. Conf. (PSCC)*, Jun. 2016, pp. 1–7.

[36] H. Xin, Z. Li, W. Dong, Z. Wang, and L. Zhang, "A generalized-impedance based stability criterion for three-phase grid-connected voltage source converters," 2017, *arXiv:1703.10514*.

[37] Y. Liao and X. Wang, "Impedance-based stability analysis for interconnected converter systems with open-loop RHP poles," *IEEE Trans. Power Electron.*, vol. 35, no. 4, pp. 4388–4397, Apr. 2020.

[38] W. Cao, Y. Ma, L. Yang, F. Wang, and L. M. Tolbert, "D–Q impedance based stability analysis and parameter design of three-phase inverter-based AC power systems," *IEEE Trans. Ind. Electron.*, vol. 64, no. 7, pp. 6017–6028, Jul. 2017.

[39] J. A. Nelder and R. Mead, "A simplex method for function minimization," *Comput. J.*, vol. 7, no. 4, pp. 308–313, 1965.

[40] T. Hathiyaldeniye Mudiyansela, B. Bagen, and U. Annakkage, "Dynamic simplifications for facilitating large power system simulations," *CIGRE Sci. Eng.*, vol. 21, pp. 116–131, Mar. 2021.

THILINI HATHIYALDENIYE (Member, IEEE) received the B.Sc. (Eng.) degree from the University of Peradeniya, Peradeniya, Sri Lanka, in 2014. She is currently pursuing the Ph.D. degree with the University of Manitoba, Winnipeg, MB, Canada. She is working as a Power Systems Engineer with Hatch Ltd. Winnipeg.

CHANDANA KARAWITA (Senior Member, IEEE) is a Professional Engineer with both industrial and academic experience in power systems. He joined TGS in 2007 while doing his doctoral research at the University of Manitoba. He is well experienced in systems planning studies related to HVAC, HVDC, and FACTS devices. He is also involved in state-of-the-art custom model development for HVDC and FACTS in both transient stability (PSSE and PSLF) and electromagnetic transient simulation (PSCAD) platforms. He actively contributes to various CIGRE working groups related to HVDC and FACTS, and is involved in academic research activities as an Adjunct Professor with the University of Manitoba.

BAGEN BAGEN (Senior Member, IEEE) received the M.Sc. and Ph.D. degrees from the University of Saskatchewan in 2002 and 2005, respectively. He joint Manitoba Hydro in September 2005. Currently, he is the Head of the Network Reliability Planning Section with the System Planning Department of Manitoba Hydro. He is an Adjunct Professor with the Electrical and Computer Engineering Department, University of Manitoba. He has authored/coauthored numerous technical papers to advance industry knowledge in the areas of probabilistic assessment of power systems, power systems analysis, and the utilization of renewable energy in power systems. He is the Canadian Representative of the International Technical Advisory Committee of the Probabilistic Method Applied to Power Systems and a Registered Professional Engineer with the Association of Professional Engineers and Geoscientist of the Province of Manitoba.

NALIN PAHALAWATHTHA (Member, IEEE) received the B.Sc. (Eng.) degree from the University of Moratuwa, Sri Lanka, in 1981, and the Ph.D. degree from the University of Calgary, Canada, in 1988. For over 30 years, his experience covers responsibility for the operation, medium, and long-term planning of the HV electricity transmission networks including planning of new load, generation, and distribution networks connections. He also has experience in planning and specification of ancillary services as well as development of networks and plant models. Over the last five years, he has been leading the connection planning and analysis on behalf of many renewable energy developers, including wind, solar, battery energy storage, hydro, and pumped hydro. He has been a member of several advisory panels and working groups for generation plant modeling, planning, and operation of high voltage networks, nationally and internationally.

UDAYA D. ANNAKKAGE (Senior Member, IEEE) received the B.Sc. (Eng.) degree from the University of Moratuwa, Moratuwa, Sri Lanka, in 1982, and the M.Sc. and Ph.D. degrees from Institute of Science and Technology (UMIST), The University of Manchester, Manchester, U.K., in 1984 and 1987, respectively. He has more than 30 years of experience in research and teaching. He is currently a Professor with the University of Manitoba, Canada. His research expertise is in the area of power systems dynamics and control.